

Third Harmonic Conversion

Celia Y. Ou

Advisor: Professor David A. Hanneke
May 7, 2013

Submitted to the
Department of Physics of Amherst College
in partial fulfilment of the
requirements for the degree of
Bachelors of Arts with honors

© 2013 Celia Y. Ou

Abstract

The $2s$ to $2p$ transition in ${}^9\text{Be}^+$, a useful one for cooling and detection, requires light of wavelength, 313 nm which is not provided by commercially available lasers. However, a viable option is to frequency triple a 940 nm Gaussian beam through a frequency doubling process followed by a frequency summing process. In order to build the frequency tripling system, I designed two power-enhancement cavities for second harmonic generation (doubling) and sum frequency generation processes (summing). The design involves consideration of crystal choice, phase matching, impedance matching, beam waist stability, and astigmatism. I chose to use a bis-muth borate crystal for doubling 940 nm light to 470 nm, and a β barium borate crystal to sum 940 nm and 470 nm to 313 nm. A preliminary experiment measures an unoptimized single-pass doubling efficiency to be $5.4(6) \times 10^{-5}\text{W}^{-1}$. Future work in optimizing the process should yield even higher efficiencies. In this thesis, we discuss the theory behind the design of the frequency tripling system, the observation of the successful occurrence of the doubling process and likely directions for future work.

Acknowledgements

Thank you, Professor Hanneke, for your guidance and teaching since last year's Interterm. Your patience and clarity with my questions nudged me along throughout the year. I never figured out how to work the label-maker in the lab.

Secondly, thank you, Professor Carter, for always encouraging me to do exciting things and reach far. Your words and enthusiasm have given me confidence and perspective. Without your suggestion, I might not have gotten to work with Professor Hanneke and write this thesis.

To all my professors and the staff, thank you for your teaching and mentorship.

Thank you to all my friends. You have put up with me, supported, inspired, and cared for me. My lab-mates Shenglan, Cheyenne, and Dvij made Hanneke Lab the coolest place to work in all of Merrill. Fellow physics majors, thank you for all your kind help and camaraderie. What fun times we had when we still went to problem sessions together and ordered pizza at night while doing I-Lab.

Many thanks to the Mr. Axel Schupf '57 and Schupf Scholars Program for the generous support and encouragement for self-initiated study and exploration. It has been a unique and valuable experience.

To my mother, father, and sister, I am very grateful and happy.

But wait! Many nuts to His Holy Fluffiness, the Squirrel God. Eternal gratefulness for guardianship under the most revered Patron Saint of the Chipmunks, Brave Protector of the Little Ones.

Contents

1	Introduction	1
1.1	Molecular ion spectroscopy	1
1.2	Beryllium Ion	2
1.3	Doppler cooling and ground-state cooling	3
1.4	Third Harmonic Conversion	4
1.5	Outline	5
2	Second harmonic generation theory and calculations	6
2.1	Linear material	6
2.2	Nonlinear material	8
2.3	Anisotropy and Birefringence	10
2.4	Phase matching	14
2.5	Optimal focusing	17
2.6	Impedance matching for doubling process	22
2.7	Doubling cavity geometry	27
3	Sum frequency generation theory and calculations	34
3.1	Sum frequency process	34
3.2	Sum frequency impedance matching	38
3.3	Summing cavity geometry	41
4	Data and Analysis	45
4.1	Apparatus	45
4.2	Single-pass conversion efficiency	50
5	Conclusion	54

List of Figures

2.1	SH power as a function of phase mismatch	10
2.2	Cross section of an example normal surface for 940 nm light in bismuth borate	13
2.3	Ordinary and extraordinary indices for BiBO	15
2.4	Impedance matching for Brewster-cut BiBO	25
2.5	Impedance matching for AR-coated BiBO	26
2.6	A ring cavity with a crystal oriented at Brewster's angle	27
2.7	Offset of the beam after passage through the crystal	31
4.1	From right to left, a half-wave plate, lens, crystal mount, lens, and diffraction grating	46
4.2	Input power to BiBO crystal	47
4.3	Crystal holder: Front view and 3D view	48
4.4	Path differences at a reflective grating	50
4.5	SH power versus the calibrated output power of the fiber	52

Chapter 1

Introduction

1.1 Molecular ion spectroscopy

The goal of this thesis is to produce 313 nm light by building a system of cavities that enhance the processes of third harmonic generation. The purpose of a 313 nm laser beam will be to aid in performing molecular ion spectroscopy. Due to their basic structure, atoms have been investigated more thoroughly and easily than molecules. In order to investigate the properties of molecules, we need a way to trap them, prepare initial states for them, and interact with them to obtain information about them. However, the complex (relative to atoms) structure of molecules makes it difficult to do such things. Thus, we restrict our attention to molecular ions, which we will call "target ions". The presence of charge of the target ions makes it possible to interact them with a simpler reference ion using the Coulomb force. We can also then use an ion trap to trap both ions. An article on quantum logic spectroscopy describes such a method of spectroscopy using ${}^9\text{Be}^+$ as the ref-

erence ion, which it calls the "logic ion"[1]. The logic ion should be one with a simple enough structure that state preparation, detection, and cooling are easy procedures. By performing these procedures for the logic ion, we would be performing analagous procedures for the target ion because it is linked with the logic ion in the midst of the procedures. The main advantage of this method of spectroscopy is that the target ion need not possess all the properties that make state preparation, detection, and cooling feasible, because of the presence of a logic ion that can fulfill some those properties instead.

We can confine both ions in a linear radio-frequency (RF) Paul trap. In a linear Paul trap, four rod-like electrodes provide a combination of alternating current (AC) and direct current (DC) potential in which to trap charged particles. One pair of electrodes provides the oscillating AC potential, which confines the particles radially. The other pair is segmented such that the middle segment is at low DC potential and the outer segments are at higher potentials. A charged particle in this potential well can be thought of as a quantum harmonic oscillator[2]. In addition, the logic and target ions' motions are coupled by the Coulomb force between them so that when we interact with the target ion, any changes in the target ion's state are tracked by the logic ion, and we can interact with the logic ion to find out what happened. For our purposes, the logic ion will also be ${}^9\text{Be}^+$.

1.2 Beryllium Ion

The design of the triple harmonic conversion cavities is for the purpose of interacting with the beryllium ion, ${}^9\text{Be}^+$. With an atomic number of 4, ${}^9\text{Be}^+$ consists

of 4 protons, 5 neutrons, and 3 electrons. The electrons are arranged into a pair in the $1s$ state and the third in the $2s$ state. The outermost electron can make a transition from the $2s$ state to the lowest energy excited state, the $2p$ state. This transition corresponds to a photon of wavelength 313nm (of energy 3.96 eV, or of frequency 0.96 PHz). One of the applications for this transition is Doppler cooling of the ion. Depending on the application, the transition wavelength may be more precisely specified, e.g., for the energy difference between specific states within the fine and hyperfine structure[2]. The ground state, $2s$, has no fine structure so it is labeled $2s^2S_{1/2}$, but does have hyperfine structure splitting from the spin-spin interaction of the valence electron and the nucleus, which has a spin of $3/2$. The excited state, $2p$, which shows fine structure from the spin-orbit interaction, splits into $2p^2P_{1/2}$ and $2p^2P_{3/2}$. The energy difference between these two states is 197.2 GHz, and each of them further splits into its hyperfine structure.

1.3 Doppler cooling and ground-state cooling

We would like to be able to cool the logic and target ions to the ground state of motion in the trap because we will use it to pass information back and forth. In order to reach the ground state, a sequence of Doppler cooling followed by ground-state cooling (Raman sideband cooling) is necessary because Doppler cooling has a limit. This could require a separate laser for each process, but a method to cool an ion with a single laser system has been demonstrated[3]. This method makes use of a beam that is detuned off-resonance of the Doppler cooling transition and modulated for either Doppler cooling or ground-state cooling. In our case, the Doppler cooling

transition will be from $2sS_{1/2}$ to $2pP_{3/2}$. One option is to detune the beam 9.6 GHz off resonance so that if it is frequency-modulated to have sidebands of 9.6 Hz, one of the sidebands reaches the Doppler cooling transition and the beam acts as the Doppler cooling beam. When the sidebands are turned off, the beam would be off resonance and useful for Raman transitions to different hyperfine states. The ability to account for this 9.6 GHz difference factors into our design later.

1.4 Third Harmonic Conversion

The obstacle here is that lasers are not commercially available at 313nm. They are also not available at 626 nm, a wavelength that could be easily frequency doubled to 313 nm if it were available in the first place. However, we can get a diode laser at 939nm in the infrared region. By making use of large nonlinear effects of synthetic crystals, part of the infrared beam can become doubled in frequency (470nm, visible blue), then rejoined with the remaining infrared part to convert into tripled frequency light of wavelength 313nm in the ultraviolet region. This 2-part process requires a ring cavity as a power build-up cavity and a crystal each for the frequency doubling and frequency summing parts and has been demonstrated for a starting wavelength of 817nm[4]. The conversion processes need to happen in power build-up cavities because the conversion is not efficient enough to produce satisfactory power within a single pass through the crystal. A single pass results in much of the original input wavelength(s) remaining and a small fraction of the output wavelength. Thus, we need a way to recycle that unused input power until all of it converts into the output wavelength (in an ideal cavity with lossless crystal

and mirrors). A ring cavity directs this light back to its starting point so that it may pass through the crystal again repeatedly until it converts. The factors that go into the design of efficiently performing cavities include the type, cut, and orientation of crystal, mirror properties, and cavity geometry.

1.5 Outline

The next chapters cover the theory and design of the power enhancement cavities. Chapter 2 discusses crystal properties such as birefringence and nonlinearity that make it possible for such crystals as β -barium borate, bismuth borate, and lithium triborate to host frequency conversion processes. Then we explain the decisions for the beam and optics properties that accounted for phase matching, optimal focusing, and impedance matching. We see that after repeating this part of the design process for each type of crystal under consideration, bismuth borate emerges as a favorable choice for frequency doubling. Chapter 3 reiterates the same aspects of the design process, but for frequency summing. Next, Chapter 4 shows the preliminary results of the frequency doubling stage, where we see that frequency doubling does occur in the crystal, as the design intended, and we measure an unoptimized conversion efficiency of $5.4(6) \times 10^{-5} \text{W}^{-1}$, which is a lower bound for the optimized efficiency. Last of all, Chapter 5 concludes with suggestions for future work.

Chapter 2

Second harmonic generation theory and calculations

2.1 Linear material

We first discuss what happens when a plane wave travels through a linear medium. A Gaussian laser beam is not a plane wave, but when its waist passes through a small crystal, it can be approximated by a plane wave around its waist, and that is what we are concerned with. Passing a Gaussian beam through a medium amounts to imposing an oscillating electric and magnetic field in the space of the medium. When an electric field is present in a medium, such as a crystal, it induces a polarization in the medium by affecting the placement of bound charges in the structure of the material. As in Eq 2.1, the polarization P is linear with the electric field E by a constant. This constant is the linear electric susceptibility, χ .

$$\vec{P} = \epsilon_0 \chi \vec{E} \quad (2.1)$$

Then, we see that the electric displacement D is

$$\begin{aligned} \vec{D} &= \epsilon_0 \vec{E} + \vec{P} \\ &= \epsilon_0 (1 + \chi) \vec{E} \\ &= \epsilon \vec{E} \end{aligned}$$

where ϵ is the permittivity of that medium. The speed at which light travels through the medium, and thus the index of refraction, depends on χ . The behavior of the electric and magnetic fields must satisfy Maxwell's equations in the absence of free charges or currents [5]:

$$\nabla \times \vec{H} = \frac{\partial \vec{D}}{\partial t} \quad (2.2)$$

$$\nabla \times \vec{E} = -\frac{\partial \vec{B}}{\partial t} \quad (2.3)$$

Taking the curl of Eq 2.3,

$$\nabla(\nabla \cdot \vec{E}) - \nabla^2 \vec{E} = -\nabla \times \frac{\partial \vec{B}}{\partial t}$$

Since the divergence of E is zero, substituting Eq 2.2 for $B = \mu_0 H$ (applicable because of the negligible magnetization for most media) in $\nabla \times \frac{\partial B}{\partial t}$ above gives

$$\nabla^2 \vec{E} = \mu_0 \epsilon \frac{\partial^2 \vec{E}}{\partial t^2}$$

Here we see that the speed, v , of the wave solution is

$$v = \frac{1}{\sqrt{\epsilon \mu_0}}$$

and so as mentioned before, the index of refraction is related to χ which is embedded in ϵ .

2.2 Nonlinear material

However, in certain media, the electric susceptibility χ has in addition to the linear constant, a nonlinear susceptibility that depends on E . We will see that this nonlinearity leads to higher harmonics of the input wave. The induced polarization in the medium is the sum of a linear and nonlinear part (Eq 2.4). If E_{source} is the electric field that drives the nonlinear polarization, the polarization is

$$\vec{P} = \epsilon_0 \chi_{linear} \vec{E}_{source} + \vec{P}_{nonlinear} \quad (2.4)$$

where $\vec{P}_{nonlinear}$ is the quadratic term of the interaction of the input E_{source} with the crystal. For i, j , and k running over x, y , and z ,

$$P_{nonlinear}^{\vec{i}} = \sum_{j,k} \hat{d}_{i,j,k} E_{source,j} E_{source,k} \quad (2.5)$$

Substituting Eq 2.4 into Eq 2.2, then into Eq 2.3 and taking the curl, we get

$$\nabla^2 \vec{E} - \mu_0 \epsilon \frac{\partial^2 \vec{E}}{\partial t^2} = \mu_0 \frac{\partial^2 \vec{P}_{nonlinear}}{\partial t^2} \quad (2.6)$$

Eq 2.6 is solved if \vec{E} is a plane wave of twice the frequency of the \vec{E}_{source} [5]. Thus when light passes through a medium with significant enough nonlinearity in its susceptibility, such as a nonlinear crystal, the light interacts with the medium, which then radiates light of twice the original frequency. This process is second harmonic generation. It turns out that if we integrate all the plane waves that result from interaction of the length of a finite crystal, then we see that the amount of SH power that finally exits the crystal depends on $\frac{\sin^2(\Delta k L/2)}{(\Delta k L/2)^2}$, where L is the distance traveled in the crystal (spanning the length of the crystal), and $\Delta \vec{k} = \vec{k}_2 - 2\vec{k}_1$ for the propagation vectors \vec{k}_1 and \vec{k}_2 of the fundamental and SH, respectively. Fig 2.1 shows us that SH power is maximized for $\Delta k L = 0$, which means that $\vec{k}_2 = 2\vec{k}_1$. The importance of the relationship between \vec{k}_1 and \vec{k}_2 comes from the fact that the newly converted SH at each point may or may not be in phase with the SH already converted prior to that point, depends on wave velocities of the fundamental and SH. Since a k-vector is $k = \frac{n\omega}{c}$, we have

$$\frac{n_2 \omega_2}{c} = 2 \frac{n_1 \omega_1}{c} \quad (2.7)$$

$$\frac{n_2 (2\omega_1)}{c} = 2 \frac{n_1 \omega_1}{c}$$

$$n_2 = n_1$$

The indices of refraction n_1 and n_2 must be the same, so the fundamental wave travels at the same speed as the SH wave, and we say that the SHG process is phase

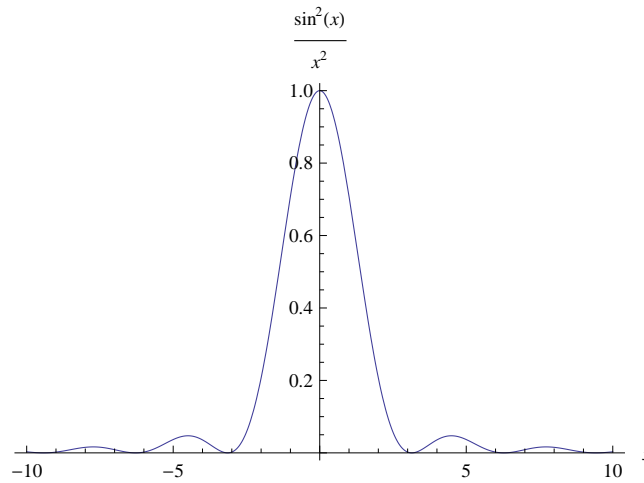


Figure 2.1: SH power as a function of phase mismatch

matched.

However, in general, such crystals exhibit chromatic dispersion, that is, n varies with the frequency of the light. In order to have $n_1 = n_2$, we employ a technique called birefringent phase matching, which requires that the crystal have more than one index of refraction, a property called birefringence. To see how a material can be birefringent, we go back to considering the material as a linear dielectric.

2.3 Anisotropy and Birefringence

If the linear permittivity ϵ is a constant tensor (called the dielectric tensor) as in Eq 2.8, then it is possible for the index of refraction to take on different values depending on the direction of E .

$$\begin{pmatrix} D_x \\ D_y \\ D_z \end{pmatrix} = \begin{pmatrix} \epsilon_{xx} & \epsilon_{xy} & \epsilon_{xz} \\ \epsilon_{yx} & \epsilon_{yy} & \epsilon_{zx} \\ \epsilon_{zx} & \epsilon_{zy} & \epsilon_{zz} \end{pmatrix} \begin{pmatrix} E_x \\ E_y \\ E_z \end{pmatrix} \quad (2.8)$$

The dielectric tensor is always symmetric, and thus diagonalizable so that if we orient our x, y, and z axes along the eigenvectors, then there are really only 3 permittivities, which are the 3 nonzero elements of the tensor [5]. The corresponding 3 indices, n_x , n_y , and n_z for electric fields in the x, y, and z directions are called the principal indices of refraction. If each element in the diagonalized tensor is the same, then the equation reduces to the case of ϵ being a single constant, and we say the medium is isotropic and has a single index of refraction that depends on wavelength but not the direction of propagation. Otherwise, the medium is anisotropic.

The principal indices are not the only allowed indices of refraction. Rather, they are like the basis vectors in the realm of all possible indices for that medium. Thus, in anisotropic media, the actual index of refraction depends on the polarization of the light. For example, for light propagating in the (diagonalized) z direction, it can be polarized with components in the x and y directions. The x component experiences an index of n_x , and the y component, n_y . One way to find all the possible indices of refraction, given the values of the 3 principal indices, is through the Fresnel equation of wave normals, which we can derive from Maxwell's time-dependent equations for a plane wave [5]. The Fresnel equation relates n , an allowed index of refraction, to the principal indices and the unit vector \hat{k} of the direction of wave propagation, expressed in its components \hat{k}_x , \hat{k}_y , and \hat{k}_z .

$$\frac{\hat{k}_x^2}{n^2 - n_x^2} + \frac{\hat{k}_y^2}{n^2 - n_y^2} + \frac{\hat{k}_z^2}{n^2 - n_z^2} = \frac{1}{n^2} \quad (2.9)$$

For \hat{k} making a polar angle θ with the z-axis and azimuthal angle ϕ from the x-axis, the Fresnel equation takes the form of Eq 2.10.

$$\frac{(\sin \theta \cos \phi)^2}{n^2 - n_x^2} + \frac{(\sin \theta \sin \phi)^2}{n^2 - n_y^2} + \frac{\cos^2 \theta}{n^2 - n_z^2} = \frac{1}{n^2} \quad (2.10)$$

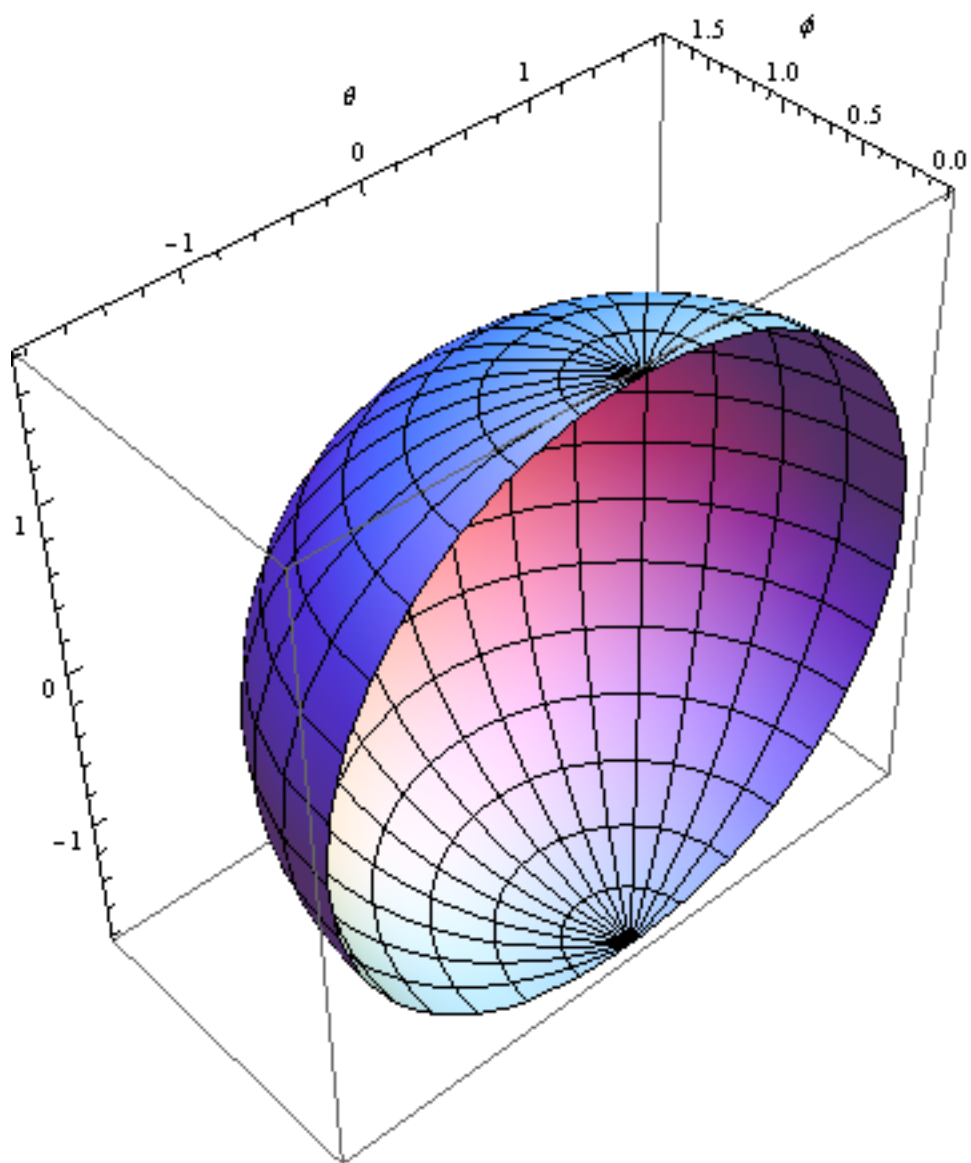
The Fresnel equation has up to 2 solutions for n . As in Fig 2.2, we can plot the refractive index n that light propagating in the direction \hat{k} would experience. Such a plot is called a normal surface. An important note is that \hat{k} is the propagation direction of the wave fronts, and so \vec{k} is the phase velocity. On the other hand, the direction of energy propagation, also called the ray direction, is perpendicular to the normal surface. Thus, the ray direction is different from \hat{k} for most values \hat{k} in an anisotropic crystal.[5]. The difference between the ray direction and phase propagation direction is called the walk-off angle, as the energy of the ray "walks off" from the wave fronts.

Another way to visualize the indices of refraction is the index ellipsoid, which Nagourney emphatically notes is different from the normal surface. This ellipsoid is a surface of constant energy density in the medium, over a range of directions of polarization (i.e., directions of E and thus D). Eq 2.11 describes the coordinates (x,y,z) of the ellipsoid [5].

$$\frac{x^2}{n_x^2} + \frac{y^2}{n_y^2} + \frac{z^2}{n_z^2} = 1 \quad (2.11)$$

The index ellipsoid is convenient in that it quickly indicates the direction of

Figure 2.2: Cross section of an example normal surface for 940 nm light in bismuth borate



polarization that corresponds with a particular index of refraction. The \hat{k} vector is placed at the origin and measured from x and z axes using the previous definitions of θ and ϕ . The plane that is perpendicular to \hat{k} intersects with the ellipsoid in an ellipse. For electromagnetic waves, the electric and magnetic field vectors are perpendicular to the direction of travel, \hat{k} . Thus, the orthogonal basis vectors for possible directions of \vec{E} are along the semimajor and semiminor axes of the ellipse, and the length of either axis is the n experienced by light with \vec{E} polarized in the direction of that axis. There are 2 categories of anisotropy: uniaxial and biaxial. Uniaxial crystals are ones for which 2 of the principal indices are the same, and so only when \hat{k} is in the z-direction does the ellipse of intersection become a circle. When this happens, n is the same no matter what the direction of polarization is. For biaxial crystals, none of the principal indices are the same, so there exist 2 possible directions of \hat{k} for which the ellipse of intersection is a circle [5]. In both cases, the optical axes of the crystal are defined to be along these special directions of \hat{k} (hence, the terms "uniaxial" and "biaxial" refer to the number of optical axes for the crystal).

2.4 Phase matching

To phase match, we determine how n varies with wavelength and counter the effect of chromatic dispersion with that of birefringence. Experimentally derived equations called the Sellmeier equations give n_x , n_y , and n_z as functions of wavelength λ . We now describe a case of phase matching that falls under the category of type-I critical phase matching, in which the two input beams are polarized in the

same direction, and the phase matching is done by tuning the angle of the crystal orientation, not by tuning temperature. Take for instance, a crystal of bismuth borate (BiBO). For a biaxial crystal like BiBO, we choose the direction of propagation to be in either the x-y, y-z, or z-x planes, (i.e., setting either θ or ϕ to be 0 or $\frac{\pi}{2}$), because it is in such directions that of the two solutions for n , one of will be ordinary and the other extraordinary. The ordinary index is the one that stays constant with respect to changes in the direction \hat{k} , while the extraordinary index is the one that does change. For a biaxial crystal, neither solution for n is solely ordinary or extraordinary for arbitrary \hat{k} with any direction of change. However, if \hat{k} lies in any of the x-y, y-z, or x-z planes that define the symmetry of the crystal's index ellipsoid, then for changes of direction strictly in either the θ or ϕ direction (but not both), we find that one solution is ordinary and the other, extraordinary.

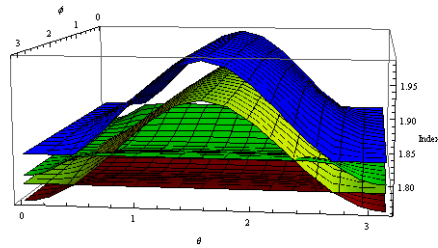


Figure 2.3: A Cartesian graph of the index as a function of propagation angle for a crystal of bismuth borate. The red and yellow solutions belong to the fundamental and the green and blue belong to the SH.

In Fig 2.3, we plot the two solutions each for wavelengths of 940 nm and 470 nm in three dimensions as functions of θ and ϕ to see which are the ordinary and extraordinary indices. Out of the two solutions that we see have points of intersection, one belongs to one wavelength and is ordinary, and the other belongs to the other wavelength and is extraordinary when \hat{k} is at those points of intersection. So

for BiBO, we set ϕ to be $\frac{\pi}{2}$ so that we are propagating in the y-z plane. For changes in θ , the fundamental solution is extraordinary while the SH solution is ordinary. Then, we set

$$n_{\lambda_1,ordinary}(\theta) = n_{\lambda_2,extraordinary}(\theta) \quad (2.12)$$

where $n(\theta)$ is the index as a function of angle θ . For frequency doubling, setting ΔkL to zero requires that $2\vec{k}_1 = \vec{k}_2$, which means the indices of refraction need to be made equal from both the effects of dispersion and double refraction. Solving for θ , we now have the direction of propagation and index of refraction of the input and output beams in the crystal. For \hat{k} at $\theta = 18.7^\circ$ and $\phi = 90^\circ$, the index of refraction for both wavelengths is 1.80. Our input and output beams are polarized perpendicular to each other. An alternative to birefringent phase matching is temperature-tuning, where the crystal is kept at a constant, elevated temperature at which temperature effects have altered the wavelength dispersion behavior so that propagation along an optical axis leads to equal fundamental and SH indices. Temperature-tuning is called non-critical phase matching and incurs no walk-off angle. Walk-off is undesirable because it adds interference between portions of SH that were generated at different points along the crystal, interference that is not fixed by phase matching. However, temperature-tuning only works for certain wavelengths in certain crystals, often at high temperatures that require careful maintenance. We would prefer to temperature-tune, but temperature-tuning conditions are not available for our choice of crystal and wavelengths. Thus, birefringent phase matching has the advantage of being more flexible and practical than temperature-tuning, despite the generation of walk-off.

2.5 Optimal focusing

Our goal is to know much power we get out of the SHG process. First, we need to know how strong the nonlinear interaction is in the crystal. We could use the nonlinear susceptibility tensor for a crystal, but the effective nonlinear coefficient d_{eff} is easier to use and find. Crystal makers often give quotes of the d_{eff} of their crystals. However, one must be cautious that d_{eff} 's differ by and must be calculated according to the direction of \hat{k} . Eq 2.13 shows that for SHG, the two input beams are both the fundamental, and so SH power has a squared dependence on fundamental power.

$$E_{SH} = d_{eff} E_{in,1} E_{in,2} = d_{eff} E_{in}^2 \quad (2.13)$$

Now that we are phase matched, the next question is, how should we focus the beam power in the crystal to get the most SH power out of the interactions in the crystal? We want to place the waist of the beam in the crystal because the waist is where the power is concentrated in the smallest cross-sectional area possible for that particular beam, and the beam is symmetric across the waist. However, if we focus too tightly, i.e., the beam waist is too small, then the Rayleigh range becomes large, meaning the the beam diverges more quickly. In this case, the power will not be concentrated around the propagation axis for a very long distance from the waist, so we get weak nonlinear interactions occurring in much of the crystal. Basically, the only useful conversion occurs in a small volume of the crystal where the waist is tight. If we focus too loosely with a large waist in the crystal, then the beam power fills out the crystal more evenly, but overall, there is no strong field anywhere

in the crystal. Boyd and Kleinman (BK) treat the calculation of SH power and optimization of focusing in a classic paper[6].

BK's approach is to input a circular Gaussian and calculate the SH power created (actually, converted) at all parts of the path traveled through the crystal, propagate them through to the end of the crystal, and add them together. Note that BK do this in Gaussian units. I have found a text that treats this in SI units and gives a supplementary explanation of the derivation of the SH power [7]. A notable aspect of their calculation is how they account for double refraction. Double refraction is the separation of the energy propagation direction (Poynting vector) from the phase propagation direction (\hat{k}). It comes from the anisotropy of the crystal. We see this in calcite, a common birefringent crystal. Looking at text through a piece of calcite, you can see two images. One image comes from ordinary rays propagating through the crystal, and the other from extraordinary rays. They traveled in the crystal at their own velocities, and the energy of the extraordinary one walked off some angle from \hat{k} , so we see its image emerge from the crystal offset from the ordinary one. In the SHG process, the effect of this is that the fundamental and SH beams separate from each other at an angle called the walkoff angle, which we introduced in Section 2.3.

To find the walkoff angle, we first find the double refraction angle ρ . This is the angle that the ray vector (Poynting vector) deviates from \hat{k} . We utilize the fact that the ray vector is normal to the normal surface[5]. Only the extraordinary ray (for us, the second harmonic) has different energy propagation and phase propagation directions. Thus, the walkoff angle (difference in direction from the two beams' Poynting vectors) comes entirely from the extraordinary ray, whether it happens to

be the fundamental or second harmonic beam. The walkoff angle is really just ρ . For our case in BiBO, ρ is 2.37° .

Now the walkoff angle is an input value into the power function from BK's 1968 paper. This h-function recasts physical quantities like crystal length, walkoff angle, and waist size into dimensionless quantities. It is an integral of all the SH contributions from infinitesimal slices of the crystal. Eq 2.15 applies for SHG in uniaxial crystals, but also applies to special cases in biaxial crystals, such as ours. The SH power is proportional to the square of the fundamental power, P_1 , and to the h-function, which accounts for the effects of focusing in a crystal with walk-off, and to other constants included in C (Eq 2.14).

$$P_2 = hCP_1^2 \quad (2.14)$$

For the biaxial crystal BiBO, our choice of \hat{k} results in one ray walking off from the other ray that stays aligned with \hat{k} , as opposed to the more general case of both rays walking off from \hat{k} .

$$h(B, \xi, \sigma) = \frac{1}{4\xi} \int_{-\xi}^{\xi} \int_{-\xi}^{\xi} \frac{e^{i\sigma(x-y) - \frac{B^2(x-y)^2}{\xi^2}}}{(1+ix)(1-iy)} dx dy, \quad (2.15)$$

where $B = \frac{\rho}{2\sqrt{Ln_1k_1}}$, $\xi = \frac{L}{2z_{opt}}$ and $\sigma = \delta kL$.

We simplified BK's equation into Eq 2.15 by taking absorption in the crystal to be zero, as we should be using crystals for which absorption is minimal in our wavelength. This is also convenient because commonly accepted absorption coefficients are difficult to find or verify. For a given length of crystal, we can optimize the h-function to find the waist size in the crystal that gives the optimum focusing.

This focusing is not too weak as to make conversion ineffective, nor too strong as to use too little of the crystal or diverge too quickly. B accounts for double refraction in the crystal. If the crystal is shorter, or the double refraction angle is greater, then B is larger, and the h-function evaluates to less than its global maximum. This is consistent with the idea that double refraction makes the use of the crystal less efficient. Note that double refraction offsets the SH power at each slice of the crystal, so the output is no longer Gaussian. ξ balances the tightness of focusing with the crystal length. The mismatch parameter, σ is the quantity that involves the k-vector difference. For focused Gaussian beams, there is an effective k-vector for the fundamental, so the optimal phase matching condition is not $2\vec{k}_1 = \vec{k}_2$ but for a small nonzero σ [8].

The optimization with respect to σ is calculated assuming that in practice σ is adjustable by tilting the crystal. ρ gives us B , so we optimize σ for all values of ξ , then optimize ξ , and use the B and optimal ξ values to find whatever σ ends up being, which can be achieved in experiment by adjusting the crystal angle slightly. Then, using the value of the h-function evaluated at these optimal quantities, we get an expression for second harmonic power as a function of fundamental power. The h-function actually evaluates to a complex number with a small imaginary part, so for ease of calculation, we take the real part of the h-function. In our case, we select a crystal length of 1 cm. At this length, we have a lot of crystal material to interact through and obtain SH power, and crystal of this size are commonly obtainable from crystal makers. Our predicted optimal mismatch parameter is 0.75, and from our optimal ξ , the target waist in the crystal should be $23.8 \mu\text{m}$. The h-function evaluates to a maximum of $h_{opt} = 0.097$.

Next, with our optimized h-function value, we calculate the maximum possible output power from a single pass through the crystal as

$$P_2 = \frac{2P_1^2 d_{eff}^2 w_1^2 k_1 L e^{-\alpha * L} h_{opt}}{\epsilon_0 c^3 n_1^2 n_2 \pi} \quad (2.16)$$

(Boyd and Kleinman), where we take α , the absorption coefficient, to be zero, since any crystal that we use should be basically transparent at the involved wavelengths. Our effective nonlinearity is $d_{eff} = 3.36 \frac{\text{pm}}{\text{V}}$.¹ Eq 2.16 has been adjusted to be in SI units, and shows that when comparing the performance of different transparent crystals of the same length for the same conversion process, the key factors are the sizes of d_{eff} and h_{opt} (which depends on the walkoff angle).

Rearranging this equation, we can obtain the single-pass conversion efficiency, $\gamma = \frac{P_2}{P_1^2}$. Our γ turns out to be $2.4 \times 10^{-4} \frac{1}{\text{W}}$. We use this best-case scenario efficiency in the equation relating the input and output intensities in a ring cavity with the reflectivities of the mirrors.

The size of γ also helps determine what crystal to use. We considered β -barium borate (BBO), BiBO, and potassium niobate (KBNO₃), all of which have fairly high nonlinear coefficients on the order of $\frac{\text{pm}}{\text{V}}$ and higher, compared to d_{eff} 's of $10^{-1} \frac{\text{pm}}{\text{V}}$ from other well-known crystals such as lithium triborate (LBO) and ammonium dihydrogen phosphate (ADP). Of these, KBNO₃ had the highest nonlinear coefficient and ended having the highest total output power in the cavity. However, it is not as commonly available as the other BBO or BiBO, and easily shows stress-induced changes in its structure. Presently, BBO is commonly chosen and available for use

¹Effective nonlinearities were calculated by the Select Non-linear Optics (SNLO) program by Dr. Arlee Smith.

in nonlinear conversion, but it has a lower nonlinear coefficient of $2.01 \frac{\text{pm}}{\text{V}}$ and is slightly hygroscopic, meaning it is susceptible to moisture in the air. BiBO has the advantage of a higher d_{eff} and being non-hygroscopic, so we choose to use BiBO in the doubling stage.

2.6 Impedance matching for doubling process

The ring cavity multiplies the input power by keeping most of it circulating within the cavity until all of it goes through the conversion process. After selecting the crystal length and determining the optimum waist size and expected single-pass conversion efficiency, we need to impedance-match the incoming fundamental beam into the ring cavity so as to enhance the single-pass conversion efficiency. Ideally, the input mirror has a certain intensity reflectivity value for the fundamental wavelength, while all the other mirrors are perfectly reflecting for the fundamental, and the output mirror is perfectly transmitting at the second harmonic. If the input mirror were 100% reflective, then the cavity keeps all the light inside, but also does not couple in any light in the first place. If the input mirror were 0% reflective, then the cavity couples all of the light inside, but also leaks all of it back out when the light finishes one round trip back to the input mirror. Thus the input mirror needs an optimal balance of reflectivity to keep the cavity useful. In reality, the three other mirrors will be as perfectly reflecting for the fundamental as can be obtained, and the output mirror will also be largely transmissive, though not perfectly, for the second harmonic. Also, the circulating power within the cavity will have an additional amount depleted from it with each round trip the light takes because of

the power that the crystal converts each time. An equation for depleted circulation (without approximation) can be derived from consideration of loss from conversion (Eq 2.17).

$$I_2 = I_0^2 \gamma \frac{(1 - r_1^2)^2}{(1 - r_1 r_m \sqrt{1 - \sqrt{\gamma I_2}})^4} \quad (2.17)$$

where I_2 and I_0 are the second harmonic and fundamental intensities, and γ is the single-pass conversion efficiency[5]. r_1 is the field reflectivity of the input mirror. Note that in commercial contexts, power(or intensity) rather than field reflectivities are given. r_m is the field transmission coefficient remaining after taking in to account the loss in the cavity that is not due to conversion, such as those due to the other three mirrors. When we talk about the reflectivity of the mirrors as a percentage, we are referring to the power reflectivity. Assuming that each of the three "ideal" mirrors are actually 99.8% reflecting and that minimal nonconversion losses in the crystal lead to 99.8% transmission,we estimate the non-conversion power loss to be about 1% in total. This gives an r_m of about 0.995. In our lab, we have about 1.5 W of input power to work with because that is what the diode laser and tapered amplifier are capable of producing. We will try our calculations for the case of frequency doubling 1 W and using the remaining 0.5 W in the summing stage. Assuming an input intensity of 1 for I_0 , we solve the impedance-matching equation for I_2 at many values of r_1 , and then plot the SH intensity versus the input reflection coefficient.

We have a choice of either a Brewster-cut or antireflection (AR)-coated crystal, to minimize reflective loss of the fundamental off the surface of the crystal. Light incident on a Brewster face can be either s-polarized or p-polarized. The s-polarized

wave is the one with its electric field polarized perpendicular to the plane of incidence, the plane defined by the incident and reflected rays. The p-polarized wave has its electric field polarized in the plane of incidence. If a p-polarized wave is incident at Brewster's angle, then the reflection coefficient is zero, meaning there will be only the refracted wave passing through the crystal. For an s-polarized wave, the reflection coefficient is nonzero, meaning there is both a reflected and refracted wave off the surface. We need the fundamental to circulate in the cavity without Fresnel loss, so we choose the cut of the crystal such that the fundamental beam is both p-polarized and an extraordinary wave, in the case of BiBO. Accordingly, the second harmonic beam is s-polarized. At the end of the crystal where the beams exit, the initial index of refraction is that of the crystal, and the final index of refraction is that of air. The incident angle, ϕ_{in} , is the complementary angle to Brewster's angle, and the exit angle, ϕ_{out} , is Brewster's angle.

For a Brewster-cut crystal, the estimated loss (coming not from the crystal, but the mirrors) is just 1% as described. However, the fundamental and second harmonic are extraordinary and ordinary, respectively, for BiBO, and so are polarized perpendicularly. So, while the fundamental exits the crystal at Brewster's angle and thus continues on with essentially no loss of intensity, some of the second harmonic reflects off the face of the crystal instead of passing through, so its power is split. This is called a Fresnel loss since the reflectivities are governed by the Fresnel equations. Here, the fraction of power retained is 72%. The field reflection coefficients for s and p polarized waves are

$$r_s = \frac{n_i \cos \phi_{in} - n_f \cos \phi_{out}}{n_i \cos \phi_{in} + n_f \cos \phi_{out}} \quad r_p = \frac{n_i \cos \phi_{out} - n_f \cos \phi_{in}}{n_i \cos \phi_{out} + n_f \cos \phi_{in}} \quad (2.18)$$

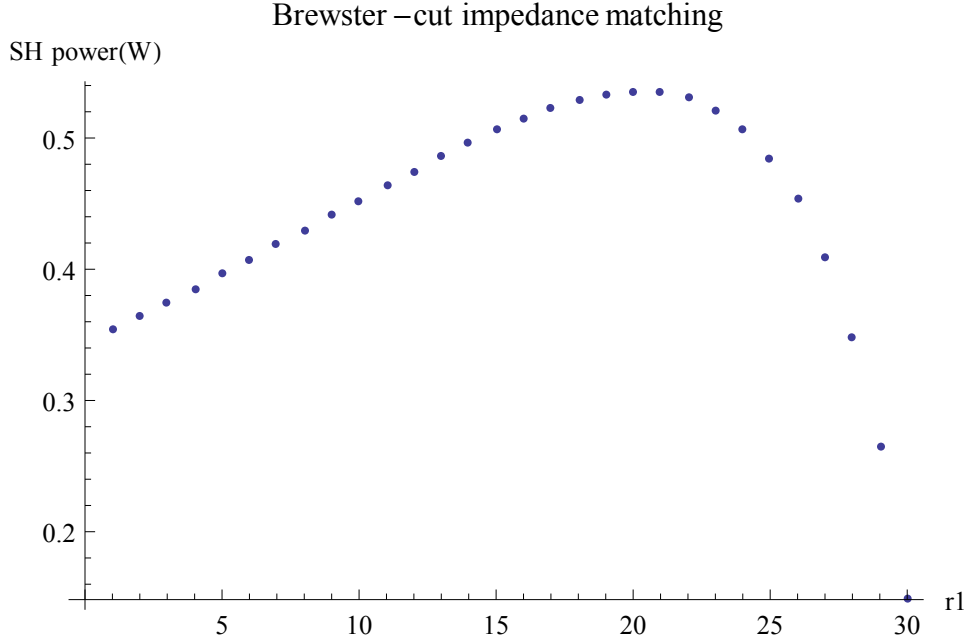


Figure 2.4: Brewster-cut BiBO: SH power versus input field reflection coefficient. The reflection coefficients range from 0.97 to 0.999 in increments of 0.001.

where ϕ_{in} is the angle of incidence relative to the perpendicular of the surface, ϕ_{out} is the exit angle, n_i is the index of refraction of the medium the beam is leaving, and n_f is the index of refraction of the material the beam is entering.

For Brewster-cut BiBO, Fig 2.4 shows the predicted output using the predicted γ and estimated losses. Our maximum output turns out to be 535 mW for an input power reflectivity of 97.8%. After taking into account the Fresnel loss of the second harmonic, the SH power that exits through the output coupler is 385 mW.

For an AR-coated crystal, the AR-coatings contribute an estimated additional 0.2% loss per surface, so for each surface, the intensity reflection coefficient is $R = 0.002$. Since $R + T = 1$, the intensity transmission coefficient is $T = 1 - R = 0.998$. Then for the two surfaces, the total fraction of intensity transmitted is

$transmitted = T \cdot T = T^2$. The total amount reflected, and therefore lost, is then $loss = 1 - transmitted = 1 - T^2$. The total loss for both surfaces turns out to be 0.4%. So, for an AR-coated crystal, we calculate the second harmonic intensity for a range of input reflectivities, but with r_m now including both the mirror and AR-coating losses, so $r_m \rightarrow r_m \cdot T^2$. Fig 2.5 shows a plot of SH power versus input reflection coefficient for AR-coated BiBO. The optimal reflectivity was similar to the Brewster-cut optimum at 97.4%, giving 420 mW of output. This is more than the end amount for the Brewster-cut, but not so much more that the slight increase is worth the cost and maintenance of the antireflection coating.

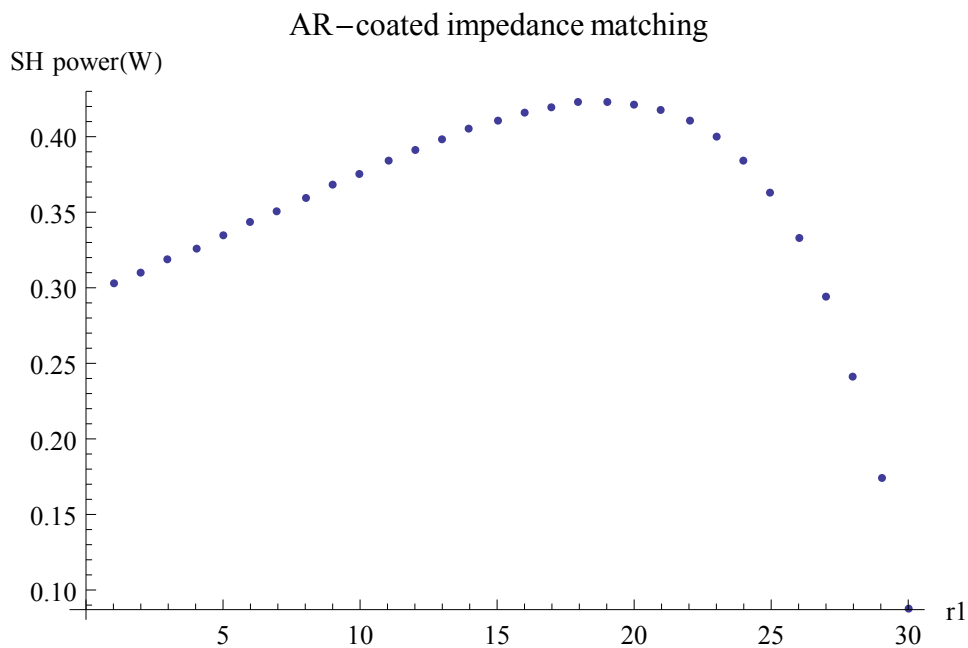


Figure 2.5: AR-Coated BiBO: SH power versus input field reflection coefficient

The plots show that if r_1 is too high, then the SH power drops off more steeply than when r_1 is too low. When γ is lower (due to absorption or sub-optimal conditions, perhaps) or r_m is higher, a slightly higher r_1 is better. Thus we should decide

on the input mirror reflectivity to be "on the safe side", that is, a little lower than calculated to be optimum, since if the reflectivity is too high, output power sharply decreases.

2.7 Doubling cavity geometry

Now, we calculate the dimensions of the cavity so that the natural mode of the cavity matches the size of the optimally focused beam that we calculated in Section 2.5. The doubling process will be performed in a ring cavity as pictured in Fig 2.6.

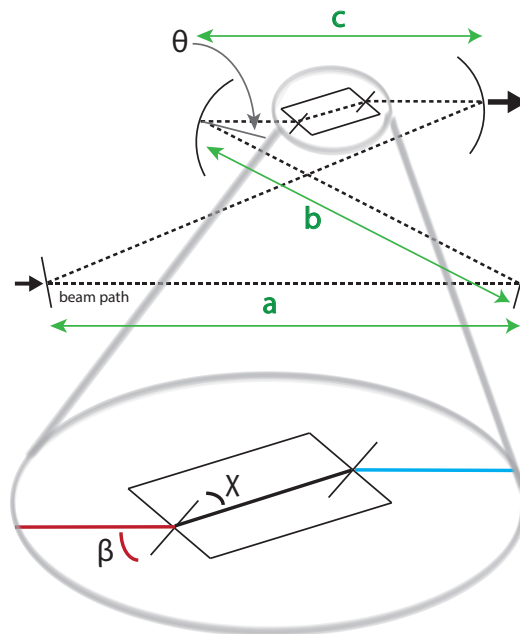


Figure 2.6: A ring cavity with a crystal oriented at Brewster's angle

Since we are working with Gaussian beams, each element of the cavity can be represented by an ABCD matrix. For all the elements put together, the two defining

characteristics of the Gaussian beam at a point in the cavity, the wavefront radius and the spot size, are described by round trip matrix. The round trip matrix is the product of the element matrices, multiplied in the reverse order of the elements encountered by the beam as it traverses one full trip around the cavity back to the starting point, the point of interest. Let's write a = long distance between the flat mirrors, b = distance from the second flat mirror to the first curved mirror, and c = distance between the curved mirrors and through the crystal, and R = radius of curvature of curved mirror. Then for the case of a ring cavity with no crystal present, and the reference point being the first curved mirror the beam encounters,

$$\begin{pmatrix} A & B \\ C & D \end{pmatrix} = \begin{pmatrix} 1 & 0 \\ -\frac{2}{R} & 1 \end{pmatrix} \begin{pmatrix} 1 & a+2b \\ 0 & 1 \end{pmatrix} \begin{pmatrix} 1 & 0 \\ -\frac{2}{R} & 1 \end{pmatrix} \begin{pmatrix} 1 & c \\ 0 & 1 \end{pmatrix} \quad (2.19)$$

For a round trip ABCD matrix, the wavefront radius and spot size at the described point are neatly given by[5]

$$R = \frac{2B}{D-A}, w = \sqrt{\frac{2\lambda|B|}{n\pi\sqrt{4-(A+D)^2}}} \quad (2.20)$$

There are two main distances, the short arm length c , and the long arm length, which is the sum $a + 2b$. If we use these to write the round trip matrix in terms of the dimensionless quantities,

$$g_1 = 1 - \frac{a+2b}{R}, \quad g_2 = 1 - \frac{c}{R},$$

or, rewriting $long = a + 2b$ and $short = c$,

$$g_1 = 1 - \frac{long}{R}, g_2 = 1 - \frac{short}{R} \quad (2.21)$$

then we can substitute Eq 2.21 into Eq 2.20. To find the waist size of the beam, we can either propagate the The square of the waist size at the center of the short arm turns out to be

$$w_0^2 = \lambda R \frac{\sqrt{g_1 g_2 (1 - g_1 g_2)}}{2n\pi g_1} \quad (2.22)$$

We now impose some constraints on the cavity parameters. One quality we want is a stable waist size with regard to changes in the arm lengths. So, we take the derivative of the squared waist with respect to *short* and set the derivative to zero. Then, solving for the short arm in terms of the long arm distance, and for the long arm in terms of the short arm, we have

$$short = \frac{2longR - R^2}{2(long - R)}, long = \frac{2shortR - R^2}{2(short - R)} \quad (2.23)$$

Next, we substitute the above expression for *long* into the one for w_0^2 , so that the squared waist is now in terms of *short* so that small changes in the short arm distance do not change the waist size at the center of where the crystal would be. Setting this new expression for the squared waist equal to the square of an actual value w_{target} of the waist calculated from second harmonic conversion theory, we obtain an equation in *short*. We then solve the equation for a goal value for the short arm length. If instead, we first substitute the equation for *long* into the one for w_0^2 and do the same thing, we obtain a goal value for the long arm length. These two target values are

$$short_0 = \frac{R\lambda_1 + 2n\pi w_{target}^2}{\lambda_1}, long_0 = R + \frac{R^2\lambda_1}{4n\pi w_{target}^2}$$

Thus, with a chosen radius of curvature, the index of refraction, fundamental wavelength, and an optimal waist size, we know what we would like the short and long arm lengths should be. For these arm lengths, the cavity is stable, that is, the cavity parameters are such that after a round trip around the cavity, the beam replicates itself so that the waist size and radius of the beam are the same as before the round trip. The condition for the beam to be stable is[5]

$$0 \leq g_1 g_2 \leq 1$$

We see that the calculated values of g_1 and g_2 from $short_0$ and $long_0$ fit the stability criterion, so we can proceed. Now, to account for the presence of the crystal, we calculate the ABCD matrix for the short arm, propagating the beam just after one of the curved mirrors through free space, the crystal, and more free space.

$$\begin{pmatrix} A & B \\ C & D \end{pmatrix} = \begin{pmatrix} 1 & \frac{c-horiz}{2} \\ 0 & 1 \end{pmatrix} \begin{pmatrix} 1 & \frac{L}{n} \\ 0 & 1 \end{pmatrix} \begin{pmatrix} 1 & \frac{c-horiz}{2} \\ 0 & 1 \end{pmatrix} = \begin{pmatrix} 1 & c - L(1 - \frac{1}{n}) \\ 0 & 1 \end{pmatrix}$$

where the horizontal distance spanned by the crystal is $horiz$ as drawn in Fig 2.7 We see that the effective short arm is then $short = c - horiz + \frac{L}{n}$. However, the length that we actually can adjust is d_0 , the distance of free space between the curved mirrors and the ends of the crystal. Thus, $d_0 = c - horiz$ and so $short = 2d_0 + \frac{L}{n}$. Substituting in the target short arm length, we find a reasonable estimate for $d_0 = \frac{1}{2}(short_0 - \frac{L}{n})$.

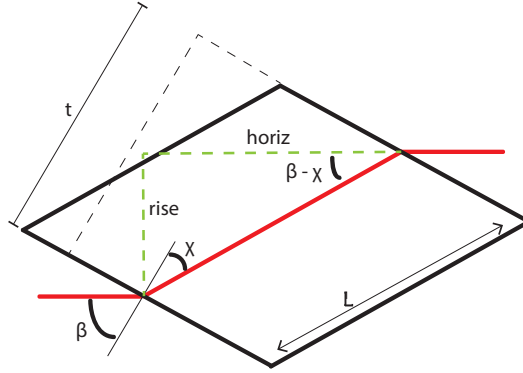


Figure 2.7: Offset of the beam after passage through the crystal

Now we deal with astigmatism in the cavity, where the beam reflects off the curved mirrors at an angle, and enters the crystal at Brewster's angle. Because the beam in the ring cavity strikes the curved mirrors and the crystal off-axis, the horizontal and vertical rays (also called tangential and sagittal, respectively) behave differently, hence the astigmatic effect. The effective length of the crystal and effective radius of curvature of mirror for the horizontal and vertical rays are denoted by subscripts h and v .

$$L_h = \frac{L}{n^3}, L_v = \frac{L}{n}$$

$$R_h = R \cos \psi, R_v = \frac{R}{\cos \psi}$$

Thus the short arm lengths are,

$$short_h = 2d_0 + \frac{L}{n^3}, short_v = 2d_0 + \frac{L}{n}$$

, using the earlier estimates of d_0 . With these, the long arm lengths, which are related by the condition set by requiring a stable waist, are

$$long_h = \frac{2short_h R_h - R_h^2}{2(short_h - R_h)}, \quad long_v = \frac{2short_v R_v - R_v^2}{2(short_v - R_v)}$$

We want to find the angle(s) for which the astigmatism from the crystal and the mirrors cancel each other in a convenient, and beneficial way, if possible. Though performing conversion with the beam having an optimal ellipticity inside the crystal leads to a greater output power than for a circular beam, we do not worry about that yet, because for the h-function for BiBO, the parameter $B \approx 7$, where $h \approx 0.1$ and the improvement from an using an optimally elliptical beam would be less than 0.05, as calculated by Freearde et al.[9]. Instead of fine-tuning the ellipticity for small improvements in conversion, we would rather look for the more experimentally simple option of inputting a circular beam into the long arm. The process of matching in an actual input beam into a cavity so that the beam's parameters match that of the cavity's natural mode, is called mode-matching. If we design the cavity to have a circular waist of a certain size in the long arm, then we must use optical elements to create the appropriate beam shape that matches the design when it enters the cavity. Mode-matching a circular beam into a circular mode is simple because no extra optics (such as cylindrical lenses) besides the spherical lenses for focusing are needed, whereas mode-matching a circular beam into an elliptical mode requires the extra optics for reshaping and as a result suffers extra losses.

Since the horizontal and vertical long arm lengths need to be the same, we start by setting $long_h = long_v$ and solve for the folding angles ψ_0 that allow this to be

true. We choose the smallest angle because mirrors work most accordingly to their design the closer to normal incidence they are used. Now we fix the folding angle at the chosen mirror radius and the long arm length, and use the round-trip matrix elements to calculate the waist in terms of the distances a , b , and c . We also know that $a + 2b = \text{long}$ so we can write the waist in the crystal in terms of long and c . We plot the horizontal and vertical waists in crystal and in the long arm as functions of c and look for the c at which the large waists are equal, and so that the beam is circular in the long arm. While the calculated folding angle may not remain the optimal angle throughout these steps, it is close enough that we can fix the angle to a constant. Over a range of mirror radii values, the dimensions of the cavity vary. For BiBO, $R = 7.5$ cm seems to be a reasonable size, with the longest dimension being about 19 cm long. This works with a folding angle of 12.1° . $R = 5$ cm is another possibility since it results in a smaller cavity of 8 cm width, which may be more difficult to realize, but should be more stable in the face of temperature changes and sound perturbations to the apparatus. In short, to choose the mirror radius value, we consider the merits and disadvantages of the folding angle and cavity dimensions that result from that choice of radius.

Chapter 3

Sum frequency generation theory and calculations

3.1 Sum frequency process

After the fundamental beam is converted into the second harmonic beam in the doubling cavity, it rejoins the remaining part of the fundamental light in the summing cavity, where the second harmonic and fundamental beams add to make a third harmonic. Sum frequency generation (SFG) is really the more general category of which SHG is the special case of summing identical beams - the fundamental beam and itself. When dealing with two input beams of different wavelengths, SFG becomes more complicated than SHG because the theory needs to account for parameters in each wavelength and the experimental apparatus must be able to couple in and circulate two beams of different wavelengths and waists in the same cavity. A design that couples both beams in but is resonant for only one beam is a simpler and

more flexible design, but limited in output power because the non-resonant beam would be in the situation of a single-pass conversion, rendering much of the build-up of the resonant beam useless. Thus a doubly-resonant cavity is more desirable than a singly-resonant one.

The summing cavity is set up in the same way as the doubling cavity, except that the second harmonic is coupled in through the second plane mirror. The reflectivities of all the mirrors and the radius of curvature of the spherical mirrors are not necessarily the same as those in the doubling cavity. The BiBO previously chosen for doubling is not transparent at 313 nm, so we chose to use a BBO crystal because it is a commonly used and effective crystal with a transparency range running from 940 nm to the third harmonic, 313 nm. BBO is a negative uniaxial crystal, so the input beams are ordinary and the output is extraordinary. We first find the waist sizes and crystal length that optimize single-pass conversion and estimate the efficiency of this conversion, then use that estimation to design the ring cavity in which to make both beams resonant.

Just as in SHG, SFG needs to be phase matched. The phase matching condition of Eq 3.1 implies that the indices of refraction for the input and output beams in the crystal must be the same. For ordinary beams of 940 nm and 470 nm summing to 313 nm in BBO, the index of refraction is 1.657, as calculated from the Sellmeier equations for BBO.

$$\Delta k = (k_1 + k_2) - k_3 = 0 \quad (3.1)$$

A paper by Guha and Falk (GF) lays out a function for the output power of a sum-frequency generation process, given the crystal length L , indices of refraction,

and input beam waists and power [10]. Like BK, GF perform their analysis in Gaussian units and call their function the h-function. We optimize the h-function with respect to the input beam waists, and find that the optimum waist sizes are not necessarily equal. However, GF points to a discussion in BK that argues that if this process is performed in a cavity resonant for both frequencies, both beams must have equal confocal parameters, i.e. the square of the ratio of the waists is the ratio of the wavelengths. This same relationship is required in order to have a ring cavity resonant at both frequencies. Thus, we maximize the power function and find that the optimum waists are not vastly different from those required by the actual realization of the cavity. This tells us that we may construct a cavity resonant at both frequencies, and the single-pass conversion efficiency will be close enough to the maximum possible that when the process is enhanced by the cavity resonance, the difference between what we could have and what we do have is small.

The resulting power from the summing process in a given crystal is

$$P_3 = \left(\frac{2n_3}{n_3 + 1}\right)^2 \frac{64\pi^2 \omega_3^2 d^2}{n_1 n_2 n_3 c^3} P_1 P_2 \frac{k_1 k_2}{k_1 + k_2} l h$$

where

$$h = \frac{1}{4\xi_4} \int_0^1 \int_0^1 \frac{e^{i\Delta k l(z_1 - z_2)} e^{-\frac{4B^2}{\alpha}(z_1 - z_2)^2 f}}{(z_1 - A_1)(z_2 - A_1^*) + C_1} dz_1 dz_2$$

for which

$$\Delta k = k_1 + k_2 - k_3, \quad k = \frac{k_1}{k_2},$$

$$B = \frac{\rho}{2} \left[\frac{l(k_1 + k_2)}{2} \right]^{1/2},$$

$$\xi_1 = \frac{l}{b_1}, \quad \xi_2 = \frac{l}{b_2},$$

$$\xi_3 = \frac{\xi_1 \xi_2 (1+k)}{\xi_2 + k \xi_1}, \quad \xi_4 = \frac{\xi_1 + k \xi_2}{1+k},$$

$$\alpha = \frac{\xi_1 + k\xi_2}{(1+k)\xi_1\xi_2},$$

$$A_1 = \frac{1}{2} + \frac{i}{4}\left(\frac{1}{\xi_3} + \frac{1}{\xi_4}\right), \quad C_1 = -\frac{1}{16}\left(\frac{1}{\xi_3} - \frac{1}{\xi_4}\right)^2, \quad z'_3 = \frac{1}{2} + \frac{i}{2\xi_3},$$

$$\text{and } f = \frac{(z_1 - z'_3)(z_2 - z'^*_3)}{(z_1 - A_1)(z_2 - A_1^*) + C_1} \text{ [10].}$$

The definitions of the k-vectors and ξ are the same as in BK, and the subscripts 1 and 2 denote the two input beams. k_3 is the third harmonic k-vector, but ξ_3 and ξ_4 are just repackaging of large groups of variables. ρ is the walkoff angle of the output, and B takes care of the walkoff in relation to the two input beams. Just as in doubling, the product Δkl , the wave vector mismatch, is tuned for optimum performance by adjusting the crystal orientation. So, we can treat Δkl as a single parameter and call it σ . The power function is then a function $P_3(\xi_1, \xi_2, \sigma)$ of the fundamental and SH focusing parameters ξ_1 and ξ_2 , and dkl . Now we have two possibly different waist sizes in the crystal. Finding the values of ξ_1 and ξ_2 that make the h-function large will give values for the waists that produce efficient SFG.

To calculate the maximum value of the h-function for our crystal, we assume that for any input fundamental and SH waist sizes, we are able to adjust the crystal angle for the most output power, so in our calculations we use the optimized value, σ_{opt} for every possible instance of ξ_1 and ξ_2 . σ_{opt} is then a function of ξ_1 and ξ_2 . Then, we numerically "crawl" over the surface of this new power function $P_3(\xi_1, \xi_2, \sigma_{opt})$ to find the values of the focusing parameters that give the most power. These values are converted back into actual waist sizes for the fundamental and SH beams, and are our target waists inside the BBO crystal. A 1 cm-long crystal works best with a $w_1 = 22.6\mu\text{m}$ waist in the fundamental and a $w_2 = 21.1\mu\text{m}$ waist in the SH, which gives an h value of 0.046. However, the ratio of the fundamental to SH waists is not $\sqrt{2}$, so these waists will not be doubly resonant in a

cavity. To make them doubly resonant, we change one of the waist sizes. We choose to change the fundamental waist size by increasing it to $\sqrt{2}w_2$ because this avoids the alternative choice of decreasing an already small waist, which runs the risk of being difficult to focus so tightly. Reevaluating the h-function shows that the new h-value of 0.043 is close to optimal of 0.046. From this, the predicted summing single-pass efficiency is $\gamma = 2.0 \times 10^{-4} \frac{1}{\text{W}}$.

3.2 Sum frequency impedance matching

The impedance matching for sum-frequency generation is more complex than for frequency doubling. To obtain maximum third harmonic power, we want the summing cavity to be resonant with both the fundamental and SH frequencies. The input power, input coupler reflectivity, and cavity loss for the fundamental and SH beams are different. This section reviews the treatment of depletion and circulation in a doubly resonant cavity presented in a classic paper by Kaneda and Kubota (KK).[11] Since here the treatment of impedance matching is based on KK, we will use power reflection coefficients as KK does and not the field reflectivities discussed for the doubling impedance matching in Section 2.6.

In the doubly resonant ring cavity, the two input beams are coupled into the cavity by different plane mirrors of high but not perfect reflectivity at both frequencies and are kept circulating within the cavity by the other three mirrors which are as highly reflective as possible for the input frequencies. There are two categories of losses to the power that circulates in the cavity: single-pass conversion loss and passive loss. The single-pass conversion loss is the amount of circulating power that

leaves the cavity by conversion to the output sum frequency, which in our case is the third harmonic. We account for this loss by including the single-pass conversion efficiency γ in the equations below. In contrast, passive loss is the amount of input power that is dissipated through any other process in the cavity, e.g. absorption in the crystal and losses in the mirrors or other optical components. We account for passive losses using δ_1 and δ_2 , the fractions of power in the fundamental and SH beams, respectively, lost to the cavity within one round-trip by any process other than sum-frequency conversion. Other variables that play a part are $R_{i,1}$ and $R_{i,2}$, the input mirror power (intensity) reflectivities for the fundamental and SH, and $P_{i,1}$ and $P_{i,2}$, the input powers coupled into the cavity. The circulating powers at each frequency are $P_{c,1}$ and $P_{c,2}$.

Assuming that γ is small enough that depletion does not factor into the third harmonic power, the third harmonic power generated at each pass is

$$P_3 = \gamma P_{c,1} P_{c,2}$$

We will use this non-depletion assumption to help create the terms below for depletion. Counting in the appropriate photon ratios, we can approximate the depletions to the fundamental and SH beams as

$$\delta_1^S = \frac{\omega_1}{\omega_1 + \omega_2} \gamma P_{c,2}$$

$$\delta_2^S = \frac{\omega_2}{\omega_1 + \omega_2} \gamma P_{c,1}$$

where the superscript "S" denotes the summing process that is the source of the

depletion. Thus, the total loss per round trip is the sum of the passive and conversion losses. The fraction of power remaining after each trip is R_m such that

$$R_{m,1} = 1 - (\delta_1 + \delta_1^S)$$

$$R_{m,2} = 1 - (\delta_2 + \delta_2^S)$$

Now we can write the ratios of circulating to input power as

$$\frac{P_{c,1}}{P_{i,1}} = \frac{1 - R_{i,1}}{(1 - (R_{i,1}R_{m,1})^{1/2})^2} \quad (3.2)$$

$$\frac{P_{c,2}}{P_{i,2}} = \frac{1 - R_{i,2}}{(1 - (R_{i,2}R_{m,2})^{1/2})^2} \quad (3.3)$$

Note that because R is an intensity coefficient rather than a field coefficient, the equations differ slightly in form compared to those discussed for doubling impedance. This is a system of two equations, linked by the circulating powers. We can then try various values of input powers and solve for the resulting circulating powers and evaluate for P_3 . Our particular setup with the diode laser and tapered amplifier gives us 1.5W of total fundamental power to put into the doubling and summing processes. From the frequency doubling section, an estimated 380 mW of SH comes out of 1 W of fundamental power, and an extra 500 mW is set aside for the summing process. Following the example of KK, we estimate the *passive* losses, δ_1 to be 0.2% and δ_2 to be 0.3% for the total mirror losses associated with a cavity containing a Brewster-cut crystal, which we take to be lossless. For an anti-reflection (AR) coated crystal, we add on an additional 0.2% loss to δ_1 and δ_2 to account for imperfect performance of the coating. Maximizing the output

power from the system of equations gives optimal reflectivities of $R_{i,1} = 99.7\%$ and $R_{i,2} = 97.5\%$ for a Brewster-cut crystal. We chose a Brewster-cut for BBO because the AR-coated case does not predict significantly higher output power, and Brewster-cut faces have lower loss and easier to maintain good performance than AR-coatings that will deteriorate. Since the indices for the fundamental and SH are so similar, the two beams basically share the same Brewster angle. The predicted circulating powers are $P_{c,1} = 166$ W and $P_{c,2} = 15$ W. Fresnel reflection of the third harmonic off the exit face of the crystal leaves 77% of the total output going through the exit face. The output of 500 mW is unexpectedly high, and even after Fresnel reflection, 380 mW of usable third harmonic remains. However, $R_{i,1}$ looks suspiciously high for an input coupling mirror as it is nearly perfectly reflecting. This may stem from the chosen passive losses being small and unequal for the different frequencies, and for these particular values of input powers, placing Eqs 3.2 and 3.3 in a region where they have the above behavior.

3.3 Summing cavity geometry

The geometry of the summing cavity is more restricted than that of the doubling cavity because we want it to be doubly resonant for the fundamental and SH. The ratio of the squares of the resonant fundamental to resonant SH beam waists in the same cavity must be 2. This is results from the equation for the spot size,

$$w = \sqrt{\frac{2\lambda|B|}{n\pi\sqrt{4 - (A + D)^2}}}$$

However, we find that when we perform the same calculations as for the doubling cavity but repeated for each input frequency, we find that the Brewster's angles and the optimal folding angles are not very different from each other. Now, when we solve for cavity lengths that gives a certain fundamental waist, the resonant SH waist in that same cavity is automatically locked into a ratio with the resonant fundamental waist. However, this combination of fundamental and SH waist is not necessarily the optimal combination calculated for single-pass conversion. What we did was to choose, based on the resultant conversion efficiency, which waist was to be the one to have its true optimal value while the other waist was to be pegged to it. Suspecting the difficulty of reaching smaller waist sizes, I chose to peg the fundamental waist to the SH waist, as that gives a larger fundamental waist rather than a much smaller waist for the SH. After calculating approximate long arm lengths, we constructed ABCD matrices in order to calculate the effects of changes in geometry on the beams at the crystal and the secondary waists at both frequencies.

The target short and long arm lengths differ between the fundamental and SH wavelength by about 1% at most, so it is acceptable to choose between the values arbitrarily and calculate the cavity lengths based on that target value. For a choice of 7.5 cm radius curved mirrors, we find that a folding angle of 11.6° minimizes the ellipticity from astigmatism and that for a long arm length of 35.7 cm, c is about 9 cm. The cavity's natural mode of $31 \mu\text{m}$ and $22 \mu\text{m}$ matches the target waists of $30 \mu\text{m}$ and $21 \mu\text{m}$ for the fundamental and SH. The secondary waists are both $216 \mu\text{m}$. We have calculated the cavity parameters for circular focusing only. Conversion may be optimized by adjusting the ellipticity of the beams in the crystal, but once

again, the addition of loss-inducing optics discourages consideration of elliptically focused beams. However, this decision may change depending on the actual shapes of the input beams we get after successfully performing SHG.

Referring back to the need for a frequency-modulated beam that was mentioned in the Introduction, we now consider the free spectral range (FSR) of the cavity. The FSR is just

$$FSR = \frac{c}{L} \quad (3.4)$$

where c is the speed of light in vacuum and L is the optical path length of a round trip in the cavity (taking into account the index of refraction of the material through which the light travels). The FSR is the interval at which, scanning through frequency space, you can find resonances with the cavity. For the cavity parameters described above, the FSR is 0.579 GHz. This means that if the cavity is at resonance with some frequency, then it is also at resonance with a frequency that is an integer multiple of the FSR away from the current frequency. We would like to have the sideband detuning of the frequency modulated beam be an integer multiple of the FSR. This way, the cavity is on resonance for both the detuned beam and the beam with sidebands. If we can relax some of the constraining conditions in the cavity design, such as astigmatism compensation or stability in the waist, then we could design a cavity with such an FSR. This kind of cavity could then take as input, a 940 nm beam frequency-modulated with the desired sidebands and efficiently produce a 313 nm with the same sidebands because the original beam and the same beam with the sidebands are all resonant. We would like to have sidebands of 9.6 or 9.2 GHz, for example. The cavity described above does not have a FSR that fits into the sidebands, but if the long arm length were adjusted within a few centimeters,

then it could have an FSR that fits.

In the realization of this design, two quartz plates will sit in the long arm to account for path length differences that result from dispersion in the crystal [4]. Although phase matching leads to nearly identical indices for input and output wavelengths, in practice, there will be a slight mismatch and thus, a path difference that needs to be resolved in order to integer numbers of wavelengths for all three beams to fit in the same round trip. The quartz plates are nominally at Brewster's angle so that the plates contribute essentially no additional loss to the cavity. However, quartz also displays dispersion across these wavelengths, so the path difference arising from that dispersion counteracts the dispersion from the crystal. As we slightly adjust the angle of the plates about Brewster's angle, Fresnel reflection remains near zero while the path lengths of the three beams shift by fractions of a wavelength.

Chapter 4

Data and Analysis

We have implemented a scheme to test that our BiBO crystal works under our design and to measure the SH power that we obtain from a single pass of the fundamental beam through the crystal.

4.1 Apparatus

A seed diode laser produces 939nm light, which passes into a tapered amplifier (TA). The TA current controller displays the current that feeds the TA, which amplifies the seed laser beam up to a few watts. The output beam is not in a clean Gaussian mode, so we feed it into a single-mode fiber to filter through the TEM_{00} mode. When the TA current is about 1.5 to 3 A, the amplified beam power is linear with the TA current. At about 3 A, the TA reaches its maximum allowed output of 1.5 W.

The output beam from the fiber passes through the center of the sequence of optics pictured in Fig 4.1. Its waist emerging from the fiber is about 1.2 mm. First,

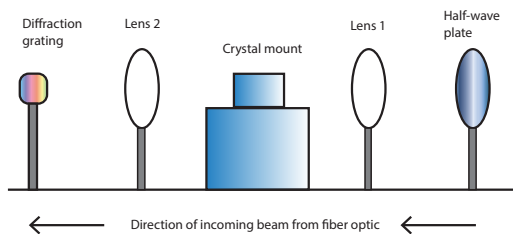


Figure 4.1: From right to left, a half-wave plate, lens, crystal mount, lens, and diffraction grating

it goes through a half-wave plate which can be adjusted to rotate the beam's polarization so that it is in the plane of the lab table (hereby called "horizontal" polarization). In our design, the horizontal polarization is the appropriate polarization for the fundamental beam to enter the crystal at Brewster's angle. Then it passes through a 10 cm focal length lens which focuses the beam down to a waist of about $25 \mu\text{m}$ at the middle of the crystal. We assume that the passage through the fiber preserves the linearity of power with current and so measure the power right after the lens. Figure 4.2 shows a linear relationship and provides calibration from the displayed TA current values to input power to the crystal.

The crystal sits in a crystal mount¹ that is bolted to a New Focus translation stage, which can adjust the mount position and angle. After leaving the crystal, the beam (which now also includes a beam of any newly converted SH light) passes through a second 10 cm focal length lens, which collimates both beams. Finally, the beams encounter a reflective diffraction grating and upon reflection, separate from each other. We place a power meter at the location of the SH beam where there

¹Modified from a design by Christian Ospelkaus (NIST)

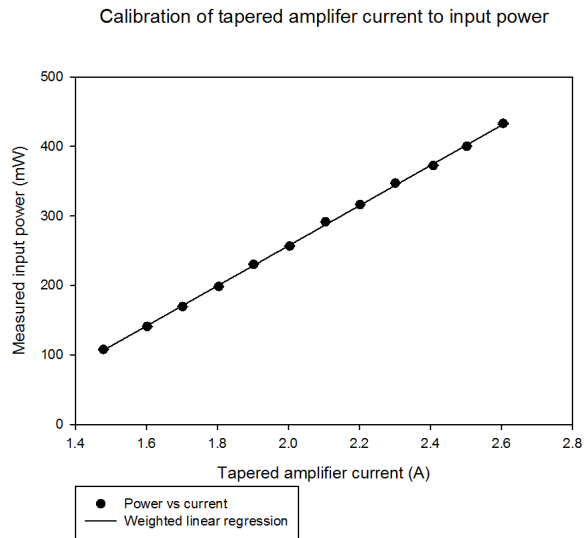


Figure 4.2: Linearity of 940 nm input power to the crystal (or, measured output power of the fiber) with TA current.

should be no fundamental reflection in order to see the expected quadratic response in the observed power to changes in the input power.

The crystal mount is designed such that if the fundamental beam is parallel to the holder's rectangular edges and enters the holder, the beam will make the correct

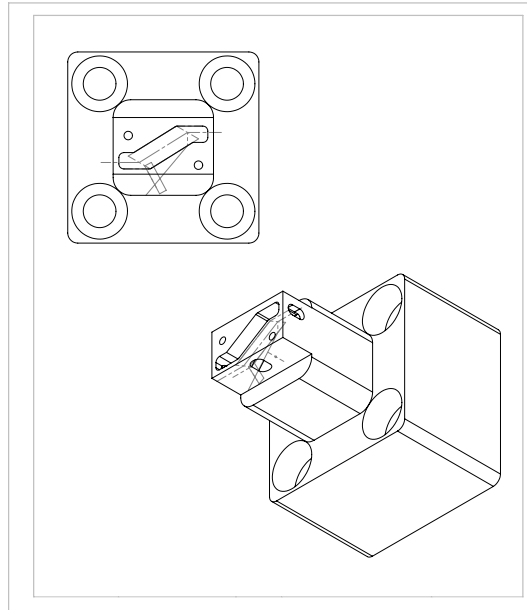


Figure 4.3: Crystal holder: Front view and 3D view

angle with the crystal's optic axis for efficient conversion, and travel successfully through the crystal and holder after obeying Snell's law at the interfaces as in Figure 4.3. To avoid additional stress-induced birefringence, we mount the crystal so that it is not gripped tightly in any direction: only the force of gravity applies force to its internal structure. The Fresnel reflection, i.e. the light that reflects off of the exit face due to its being polarized perpendicular to the lab table, refracts through the side of the crystal and exits through a hole in the mount so that the light does not reflect with the crystal uselessly and heat it up. From adjusting the degrees of freedom in the translation stage, the angle and position of the crystal is finely adjusted to maximize conversion. The mount has a cover to protect the crystal from dust and scrapes while it sits in the mount.

What we want to measure is SH power, and there is already so little of it com-

pared to the fundamental power, so we need a way to separate the fundamental and SH since in the single-pass conversion process, there are no mirrors with wavelength-dependent coatings to separate out the beams. However, we can make use of the wavelength-dependent behavior of diffraction gratings. The location and intensity of diffraction maxima depend on the wavelength, grating spacing, and grating shape. A blazed grating is one in which the grooves are not a constant depth but slant down at the *blaze angle* from one side to the other across the short dimension. When a grating is blazed for a certain wavelength, this modification concentrates the bulk of the diffracted power on the first-order maximum for that wavelength. Our diffraction grating (DG) is blazed for efficient performance at 500 nm and has 1200 grooves per mm. We are looking for the SH power so that is why the DG's design wavelength is close to the SH rather than the fundamental. The grooves of the grating are the numerous places from which the incident light reflects, and thus act like point sources. An overview of diffraction gratings can be found in various sources.²

Figure 4.4 shows a grating of groove spacing d and light from a plane wave incident at angle α from the normal to the grating plane (not the individual blazed grating surfaces). However, the "rays" marked by angle β are not rays at all. Thus reflective gratings follow the diffraction grating equation (Eq 4.1) for the m^{th} constructive interference maximum at an angle β from the normal.

$$m\lambda = d(\sin \beta - \sin \alpha) \quad (4.1)$$

What happens is that the Gaussian beam of the laser is approximately a plane wave

²An example is the Thorlabs Grating Tutorial at http://www.thorlabs.com/newgrouppage9.cfm?objectgroup_id=26

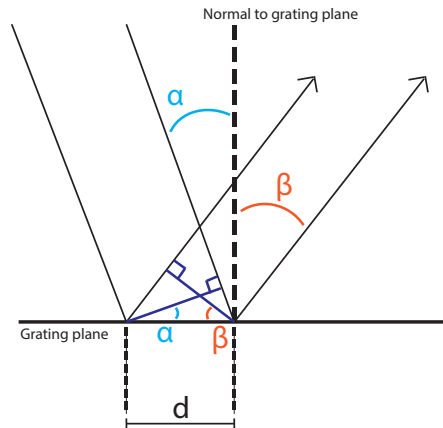


Figure 4.4: Path differences at a reflective grating

at the diffraction grating. Zoomed down at the individual blazed surfaces, each ray follows the law of reflection, but far away from the grating at various angles β , they interfere constructively and destructively with each other. Using this equation, we set up the incident angle to be 45 degrees so that from the law of reflection, the zeroth order diffraction is at a right angle to the initial beam path. We calculate the expected angles for the $m = -1$ for fundamental and SH, and confirm their positions in experiment. The 940nm light should diffract off at -24.9° and the 470 nm light at 8.2° .

4.2 Single-pass conversion efficiency

To aid in the collection of solely SH light at the power meter, I placed right in front of the power meter, a metal cylinder of a radius roughly 2 times that of the

aperture of the power meter. The beam passed through the tube to get to the power meter. This tube is to reduce the amount of room lighting that reaches the power meter. I lined the inside surface at the entrance to the tube and covered the seam between the meter and the tube with black electrical tape. Then, I placed the meter and tube at a close enough distance from the diffraction grating that when the SH beam reaches the meter, it has not spread out enough to surpass the diameter of the meter aperture, but also is far enough that the fundamental beam has separated enough spatially from the SH beam.

Thus, after using adjusting the position and angle of the crystal for maximum SH power, I varied the TA current and recorded the corresponding SH powers. I plot the SH power versus the calibrated fundamental power in Fig 4.5.

As anticipated, the relationship is quadratic, which indicates that the blue light that exits the crystal is a result of frequency doubling. A nonlinear regression to the form ax^2+bx+c , where a , b , and c are constants, gives a value of $3.8(4) \times 10^{-5} \text{W}^{-1}$, which is our single-pass efficiency, γ . However, the SH power measured does not account for all of the light that was converted into SH because the diffraction grating distributes the incident power into several orders of diffraction maxima. According to the specifications for the diffraction grating we used, the efficiency at 500 nm wavelength is 70%. From this, we infer that the amount of SH power exiting the crystal should be about $5.4(6) \times 10^{-5} \text{W}^{-1}$. This is still an order of magnitude smaller than the $2.4 \times 10^{-4} \text{W}^{-1}$ calculated in our BK analysis. I expect that several factors contribute to this sub-optimal efficiency. The first is that the we did not optimize the size of the waist. Secondly, we did not center the waist in the middle of the crystal. Centering the waist in the crystal is the best use of the focusing of the

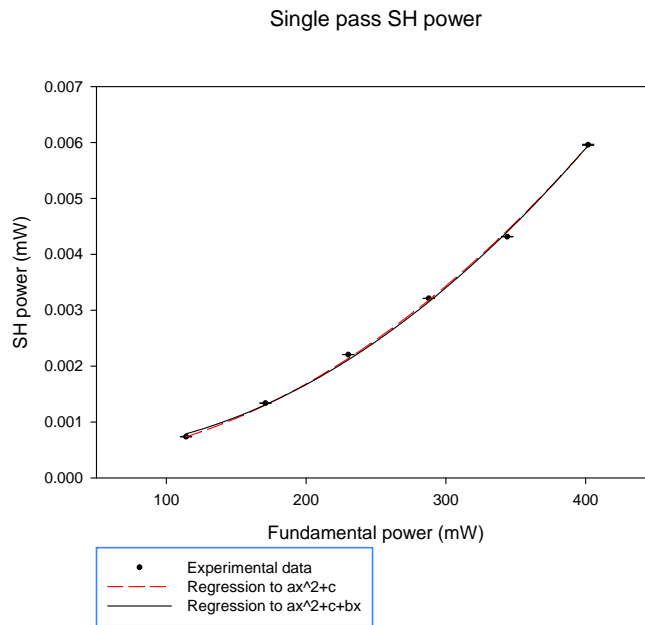


Figure 4.5: SH power versus the calibrated output power of the fiber

beam and is the situation for which we calculated γ . Third, if the output polarization of the fiber is elliptical at all, then the most that the half-wave plate could do alone is to rotate such that the majority of the light is polarized in the tangential direction.

For the purpose of measuring γ , we should have used a linear polarizer before the power detector when measuring the input fundamental power, so that we would actually measure the amount power in the correct polarization.

Chapter 5

Conclusion

So far, we have reached the first stage of converting a 940 nm beam into a 470 nm beam in a single pass through a BiBO crystal. We also have designs for the power enhancement cavities for both frequency doubling and summing. Both cavities are designed to have waists that are stable with changes in cavity length inside the nonlinear crystals, minimize the effects of astigmatism, and to be impedance matched. With the minute distances traveled in piezoelectric motion, the doubling cavity can be made resonant with the fundamental frequency and the summing cavity doubly resonant with the fundamental and SH while maintaining the waists in the crystals that give the maximum single-pass efficiencies.

There is much future work that is clearly foreseeable. The most immediate work is to properly couple in the tapered amplifier output into the single-mode fiber to give as much input power as possible exiting the fiber. We should also use a quarter-wave plate somewhere between the fiber exit and the first lens to linearize any elliptical polarization. Next, we should measure the maximum obtainable single-pass

efficiency by adjusting the waist size and position in the crystal.

The next steps to take are to build the SHG cavity, try a single-pass conversion through the BBO summing crystal, and build the summing cavity. Both cavities need work on the system of electronics that provides a feedback signal to direct the motion of a piezoelectric crystal for cavity locking to the input wavelengths. In addition, different input powers than the ones posited in calculations may result from losses in fiber coupling or frequency doubling conversion that was well under expectations. Thus, we plan to switch out the input coupling mirrors for several other mirrors with different reflectivities. This also allows us to check how well the predicted optimal reflectivity is suited for impedance matching. Lastly, we need a way to automate the determination of a cavity with the desirable FSR instead of having the program calculate the calculate cavity lengths using a guess-and-check method that requires manual input. With this design, we hope to produce usable amounts of ultraviolet 313 nm light.

Bibliography

- [1] P. O. Schmidt, T. Rosenband, C. Langer, W. M. Itano, J. C. Bergquist, and D. J. Wineland, “Spectroscopy Using Quantum Logic,” *Science* **309**, 749 (2005).
- [2] C. E. Langer, *High Fidelity Quantum Information Processing with Trapped Ions*, Ph.D. thesis, University of Colorado (2006).
- [3] B. Hemmerling, F. Gebert, Y. Wan, D. Nigg, I. V. Sherstov, and P. O. Schmidt, “A single laser system for ground-state cooling of $^{25}\text{Mg}^+$,” *Appl. Phys.B* (2011).
- [4] J. Mes, E. J. van Duijn, R. Zinkstok, S. Witte, and W. Hogervorst, “Third-harmonic generation of a continuous-wave Ti:Sapphire laser in external resonant cavities,” *Appl. Phys. Lett.* **82**, 4423 (2003).
- [5] W. Nagourney, *Quantum Electronics for Atomic Physics* (Oxford University Press, 2010).
- [6] G. Boyd and D. Kleinman, “Parametric Interaction of Focused Gaussian Light Beams,” *Journal of Applied Physics* **39**, 3597 (1968).

- [7] W. Risk, T. Gosnell, and A. Nurmikko, *Compact Blue-Green Lasers* (Cambridge University Press, 2003).
- [8] D. Kleinman, A. Ashkin, and G. Boyd, "Second-Harmonic Generation of Light by Focused Laser Beams," *Physical Review* **145**, 338 (1966).
- [9] T. Freearde, J. Coutts, J. Walz, D. Leibfried, and T. W. Hänsch, "General analysis of type I second-harmonic generation with elliptical Gaussian beams," *J. Opt. Soc. Amer. B* **14**, 2010 (1997).
- [10] S. Guha and J. Falk, "The effects of focusing in the three-frequency parametric upconverter," *Journal of Applied Physics* **51**, 50 (1980).
- [11] Y. Kaneda and S. Kubota, "Theoretical treatment, simulation, and experiments of doubly resonant sum-frequency mixing in an external resonator," *Applied Optics* **36**, 7766 (1997).